Co-published by
Institute of Fluid-Flow Machinery
Polish Academy of Sciences
Committee on Thermodynamics and Combustion
Polish Academy of Sciences

http://www.imp.gda.pl/archives-of-thermodynamics/

Exergoeconomic Optimisation of a Novel Tri-Evaporator Solar-Biomass Multigeneration System Coupled with Fuel Cell and Electrolyser

Obiora Emeka Anisiji[a,b*], Ikuobase Emovon[b], Olusegun David Samuel[b], Fidelis Abam[c]

[a]Department of Mechanical and Mechatronics Engineering, Federal University Otuoke, P.M.B. 126, Yenagoa, Nigeria
[b]Department of Mechanical Engineering, Federal University of Petroleum Resources Effurun, P.M.B. 1221, Effurun, Nigeria
[c]Department of Mechanical Engineering, University of Calabar, P.M.B. 1115, Calabar, Nigeria
*Corresponding author email: anisijieo@fuotuoke.edu.ng

Received: 17.02.2025; revised: 06.05.2025; accepted: 14.05.2025

Abstract

This study presents a novel, cost-effective multigeneration system configuration that utilises locally available solar irradiance and biomass resources to produce hydrogen, electricity, heating, hot water, and cooling. The system integrates a range of energy conversion technologies, including non-conventional parabolic trough collectors, conventional biomass gasification, the Kalina cycle, organic Rankine cycle, vapour absorption system, an electrolyser, and a fuel cell. A thermoeconomic analysis was conducted to evaluate system performance, with exergy-based costing applied to determine the operating costs while optimising overall net output. The study also assessed the exergetic sustainability of the system by analysing thermodynamic inefficiencies. It was found that an optimal ambient temperature of approximately 297.4 K maximises the system's exergetic sustainability index, reaching a value of 1.00. The levelized cost of electricity from the Kalina and organic Rankine cycle subsystems was calculated as 0.04308 USD/kWh and 0.0245 USD/kWh, respectively, corresponding to an exergoeconomic factor of 44.51%. When converted to Nigerian currency, these values equate to 69.12 NGN/kWh and 39.31 NGN/kWh – significantly lower than the prevailing electricity tariff in Nigeria, which stands at approximately 209.50 NGN/kWh (0.1306 USD/kWh). Under specified operating conditions, the optimal work outputs of the organic Rankine cycle and Kalina cycle turbines were 47.97 kJ/kg and 435.3 kJ/kg, respectively. The overall energy and exergy efficiencies of the integrated plant were recorded at 52.2% and 16.14%. This multigeneration system demonstrates strong potential as an alternative to fossil-fuel-based power generation, particularly in applications and sectors with low energy demand.

Keywords: Multigeneration; Exergy efficiency; Exergoeconomics; Optimisation; Exergetic sustainability

Vol. 46(2025), No. 3, 113–126; doi: 10.24425/ather.2025.156583

Cite this manuscript as: Anisiji, O.E., Emovon, S., Samuel, O.D., & Abam, F. (2025). Exergoeconomic Optimisation of a Novel Tri-Evaporator Solar-Biomass Multigeneration System Coupled with Fuel Cell and Electrolyser. *Archives of Thermodynamics*, 46(3), 113−126.

1. Introduction

The likelihood of exhausting conventional energy sources becomes increasingly certain in light of the recent correlation between wealth and energy usage, as well as the sharp rise in energy consumption. In addition, sudden changes in the environment brought on by the release of heat and waste materials have had a severe and unsettling impact on human life as well as endangered animal species. In this regard, global warming represents a challenge that humanity has yet to conquer. It is therefore more important than ever to discover an environmentally acceptable substitute for conventional fuels that performs as well. Renewable energy sources, such as waste heat and waste material sources, may be preferable options in this regard.

Nomenclature

c – specific cost of product
c_p – specific heat, J/(kg·K)
$\dot{C}$ – cost rate
$E_{D,Ratio}$ – exergy destruction ratio
$\dot{E}_{D_k}$ – exergy destruction rate, kJ/s
$\dot{E}_{Q_k}$ – exergy associated with heat, kJ
$\dot{E}_{W_k}$ – exergy associated with work, kJ
f – exergoeconomic factor
h – specific enthalpy, kJ/kg
H – higher operating limit
L – lower operating limit
$\dot{m}_i$ – mass flow rate, kg/s
n – estimated plant life in years
N – annual operational hours
P – pressure
$\dot{Q}_k$ – heat rate to the k^{th} component, kJ/s
s – specific entropy, kJ/(kg·K)
T – temperature
$\dot{W}_k$ – rate of work output from the k^{th} component, kJ/s
$\dot{Z}_k$ – levelised cost rate

Greek symbols

ψ_{plant} – exergy efficiency
Γ_{eef} – environmental effect factor
θ_{esi} – exergetic sustainability index

Subscripts and Superscripts

F – fuel
i – inlet
j – outlet stream
k – element, component
o – outlet
P – product
q – heat transfer
turb – turbine
w – work

Abbreviations and Acronyms

Al_2O_3 – aluminium dioxide
CMP – compressor
CON – condenser
COP – coefficient of performance
CRF – capital recovery factor
EES – engineering equation solver
ESI – exergetic sustainability index
EVP – evaporator
HEX – heat exchanger
KC – Kalina cycle
LiBr – lithium bromide water
MWCNT – multi-walled carbon nanotube
NH_3 – ammonia
ORC – organic Rankine cycle
PEC – purchase and equipment cost
PECF – purchase of equipment cost fund
PEM – proton exchange membrane
PTC – parabolic trough collector
PUM – pump
S – separator
VAS – vapour absorption system
VG – vapour generator

However, the idea of integrating systems with multiple production offers a big possibility [1]. In this regard, multiple attempts have been made to integrate diverse energy technologies in order to reduce carbon emissions while also providing a more efficient and reliable energy supply [2]. Integration, which involves connecting two or more energy technologies inside a single structure, provides advantages over their stand-alone equivalents due to the mutual utilisation of substructures and feedstock [3]. However, unique engineering methodologies, such as thermodynamic studies, should be used to analyse the efficacy of such novel integrated systems from an environmental and budgetary standpoint [4].

A multigeneration system generates electricity, heating, cooling, hot water, freshwater, hydrogen, and other energy from a single or multiple sources. The multi-generation system produces electricity using one or more prime movers, such as a gas turbine, Rankine cycle, or organic Rankine cycle (ORC). Because of its suitability for recovering energy from low-grade heat sources, the ORC is a process that might be incorporated into a multigeneration system [5]. Multi-generation systems can achieve better efficiency than single-generation systems [1]. Furthermore, it has been demonstrated that in these integrated systems, fuel consumption may be lowered by using waste heat and renewable energy. As a result, these sources have the potential to reduce emissions while also diversifying commodities [6]. The complexity of energy flows in integrated systems, such as multigeneration systems with various outputs, makes cost allocation to each product a big difficulty [7]. Researchers have used a variety of cost allocation approaches, but the thermoeconomic or exergoeconomic method is suggested due to its ability to properly calculate the costs of various items [1]. Exergoeconomic analysis is a useful method for improving the performance of multigeneration systems [8] by integrating exergy and economic analysis [9]. Several research works utilised the exergoeconomic technique to improve their systems. A thermoeconomic multi-objective optimisation was performed by Ahmadi et al. [10] on a novel integrated multigeneration system consisting of a biomass combustor, proton exchange membrane (PEM) electrolyser, organic Rankine cycle, double effect absorption chiller, domestic water heater, reverse osmosis desalination, and a heat exchanger. They observed that increasing design parameters within their maximum values enhances both the multi-objective function of the total cost rate and the system's exergy efficiency. Calise et al. [11] simulated a novel solar-geothermal-based multigeneration system producing electricity, heating, cooling and fresh water. The system is built on a combination of thermal recovery system (TRS), ORC, parabolic trough collectors (PTC) and multi-effect distillation. Their exergetic and exergoeconomic analysis results were presented on a daily, weekly and annual basis. The system cost led to s high price of electricity in the energy market. Baghernejad et al. [12] conducted an exergoeconomic optimisation and environmental analysis of

a new solar trigeneration system based on an integrated solar combined cycle system (ISCCS) (power generating unit), a cooling unit, a heating unit and an electrical generator. Optimisation results obtained show a 26.34% increase in exergy efficiency and 11.5% decrease in unit cost of products, a 24.17% decrease in fuel exergy, a 21.63% reduction of total exergy destruction and a 24.17% reduction in CO_2 emission cost. Moharamian et al. [13] performed an exergoeconomic and thermodynamic analysis of the influences of injecting hydrogen into the combustion chamber of a biomass-based externally fired combined cycle hydrogen injection (EFCCHI) and compared it with hydrogen production with no injection (EFCCH). They found that hydrogen injection into the combustion chamber reduces fuel consumption by 27%, exergy and energy efficiencies by 45% and CO_2 emissions by 32%. Also, exergy loss and destruction cost rates were reduced by 78% and 10% respectively. Khalid et al. [14] proposed a thermoeconomic analysis of a hybrid solar-biomass multigeneration system for a community comprising an absorption chiller, a solar cycle, two organic Rankine cycles and a Brayton cycle to produce electricity, hot water, cooling and heating. Their results show energy, exergy efficiencies, electricity system cost and levelized cost of electricity as 91.0%, 34.9%, $2 700 496 and $0.117/kWh, respectively. Khanmohammadi et al. [15] conducted a thermoeconomic modelling and optimisation of a multigeneration system comprising a solar flat plate collector, an organic Rankine cycle, a PEM electrolyser and a single effect absorption chiller. Their results indicate that exergy efficiency and cost of the system can simultaneously increase from 1.72% to 3.2% and 19.59 $/h to 22.28 $/h, respectively. Also, raising the evaporator temperature of the ORC unit to the upper limit increases electric power generation and increases the production rate of hydrogen from 0.23 to 0.35 kg/day but decreases the cooling capacity from 44.29 kW to 22.6 kW. A novel solar power-based polygeneration system producing electricity, fresh water, cooling, domestic hot water, and hydrogen was analysed by El-Emam and Dincer [16]. The results of the thermoeconomic and multi-objective optimisation of the system show a maximum exergy efficiency of 39% obtained at a cost rate of 309 $/h and a lowest exergy efficiency of 21.7% at a rate of 241 $/h. Khanmohammadi et al. [17] proposed and studied the thermoeconomic and multi-objective optimisation of a multigeneration structure with a thermoelectric waste heat recovery system (WHRS). The system is composed of a gas turbine cycle, an organic Rankine cycle and a domestic water heater. They obtained that the efficiencies of the system can be raised from 16.76% to 17.93% by attaching a WHRS on the ORC condenser. Behzadi et al. [18] proposed an integrated energy system composed of a biomass-based solid oxide fuel cell (SOFC) with a gas turbine, a reverse osmosis desalination unit and a double effect absorption chiller. Thermoeconomic and optimisation study results show the gasifier as the primary source of irreversibility with an exergy destruction rate of 179.8 kW; the pump and SOFC stack have the highest exergoeconomic factor at optimal operating conditions; the exergy efficiency is 38.16% and the total product unit is 69.47 $/GJ. Anvari et al. [19] proposed and conducted a thermodynamic, exergoeconomic and environmental analysis of a gas turbine cycle-based multigeneration system with absorption refrigeration cycle, ORC and desalination unit subsystems. The results of their assessment show that the overall cost and CO_2 emissions are 1943.5 $/h and 0.163 kg/kWh, respectively. For every 83.56 MW energy input into the cycle, electric power of 30.5 MW, cooling of 1MW, heat of 40.8MW and freshwater of 0.364 kg/s were generated. Also, raising temperatures of the pre-heater outlet air (800 K−1000 K) and gas turbine inlet (1320−1570 K) reduces CO_2 emissions of the cycle by 26.6% and 53%, respectively. Abdelhay et al. [20] conducted a thermodynamic analysis of a solar-based multigeneration system powered by a natural gas heater. The system layout includes a solar power cycle, a multi-effect desalination unit, and an absorption refrigeration unit, which generates electricity, fresh water, and cooling for around 1000 households. The modelling findings suggest that the maximum total system exergy efficiency is 23.95%, compared to 23.14% or less for any subsystem that is stand-alone or dual-purpose. The system also offers the lowest unit prices of water and cooling, at 1.247 $/m^3 and 0.003 $/kWh, respectively.

Alirahmi et al. [21] conducted a thermo-economic analysis and multi-criteria design optimisation of a geothermal and solar-driven multigeneration system, using the metrological data of three cities. The system layout consists of a geothermal cycle, solar cycle, Rankine cycle, thermoelectric generator, ORC, absorption chiller, desalination unit and an electrolyser, which they aimed to produce space heating, space cooling, fresh water, hot water, electric power and hydrogen. Results of their study show exergy efficiency and cost rate as 21.63% and 63.89 $/h, respectively. Also, on a typical sample day, the system produced 373.8 m^3 of fresh water and 26.38 kg of hydrogen in one city. A thermodynamic and exergoeconomic analysis of a novel solar-assisted multigenerational system utilising high-temperature phase change material and hybrid nanofluid was performed by Khan et al. [22]. Their system integrated a parabolic dish collector with hybrid nanofluids, double effect lithium-bromide/water absorption cycle, PEM electrolyser, recompression sCO_2 Brayton cycle, and a desalination unit, producing electricity, cooling, hydrogen and fresh water. Results show that fresh water and cooling productions are 1.564 kg/s and 196.1 kW, respectively, and the total energy and exergy efficiencies of the analyzed system are 31.59% and 30.02%, respectively, while the exergoeconomic results show the total cost rate of exergy destruction and levelised cost of electricity are 530 $/h and 0.1387 $/kWh, respectively.

The following evaluation objectives were taken into consideration while conducting the above thorough literature review: the architecture of the multigeneration system, the system's primary energy resources and how they are converted, the effective utilisation of energy sources for each subsystem, the method of producing hydrogen, the decarbonization of power production, the system and its primary end products. It is found that a multigeneration energy system powered by a combination of biomass and solar energy sources with PTC system running on a hybrid nanofluid (MWCNT-Al_2O_3 / therminol VP1), incorporating and utilising the tri-evaporator system has not been investigated by integrating a unique ORC system combined with

a Kalina cycle (KC), vapour absorption system, proton exchange membrane, and a fuel cell, using minimum energy of the configured system to generate electricity, heating, cooling, hot water, and hydrogen. Furthermore, the performance of linked subsystems in such a multigeneration system must be investigated under various operational conditions. It is anticipated that these systems will open up a number of new possibilities for using biomass and solar energy sources.

Inspired by these gaps in the literature, this study proposes an integrated energy system that generates clean energy from renewable sources. A key innovation lies in the use of a single working fluid to drive three interconnected subsystems. By strategically bleeding the fluid during turbine expansion, the same medium is repurposed for cooling production. This integrated design shortens the thermodynamic process path, reduces system complexity, and minimises the number of components required. As a result, it enhances overall performance, boosts energy utilisation, and achieves a higher cooling-to-power ratio – an especially noteworthy aspect of this study. Furthermore, the paper develops models for an innovative cycle featuring a tri-evaporator system. This includes a conventional evaporator in the vapour absorption system (VAS) and unconventional evaporators in both the ORC and KC subsystems. The tri-evaporator configuration provides numerous benefits, such as increased cooling capacity, improved heat recovery, enhanced flexibility, reduced temperature differentials, greater system reliability, better heat transfer, and improved overall energy efficiency. By enabling heat recovery from multiple sources, minimising thermal stress, and offering operational redundancy, this configuration represents a significant advancement in integrated energy systems.

The objectives of this research include the development of a new renewable energy-based integrated system capable of producing various utilities, economic assessment of the system in terms of the levelized cost of electricity and net present cost, asd the integrated system exergetic sustainability analysis and optimisation. To achieve this, the study involves a thorough investigation using: exergoeconomic balance equations for each system component analysing how state properties and varying operating conditions impact individual subunit performance as well as the system's overall performance; sustainability analysis with regards to total system output and the gross exergy destruction in the plant; and optimization, with respect to optimum selection of operating parameters for the ORC and Kalina turbines.

2. System description

Figure 1 depicts the suggested multigeneration design. According to the system overview, the integrated energy system's primary energy source is the solar-powered parabolic trough collector (PTC). Other energy sources include the KC unit, the ORC unit, the vapour absorption system (VAS), a proton exchange membrane (PEM) electrolyser that produces hydrogen through a biomass combustor, and a fuel cell that runs on the hydrogen produced by the PEM electrolyser. The workings of these subsystems are vividly described below.

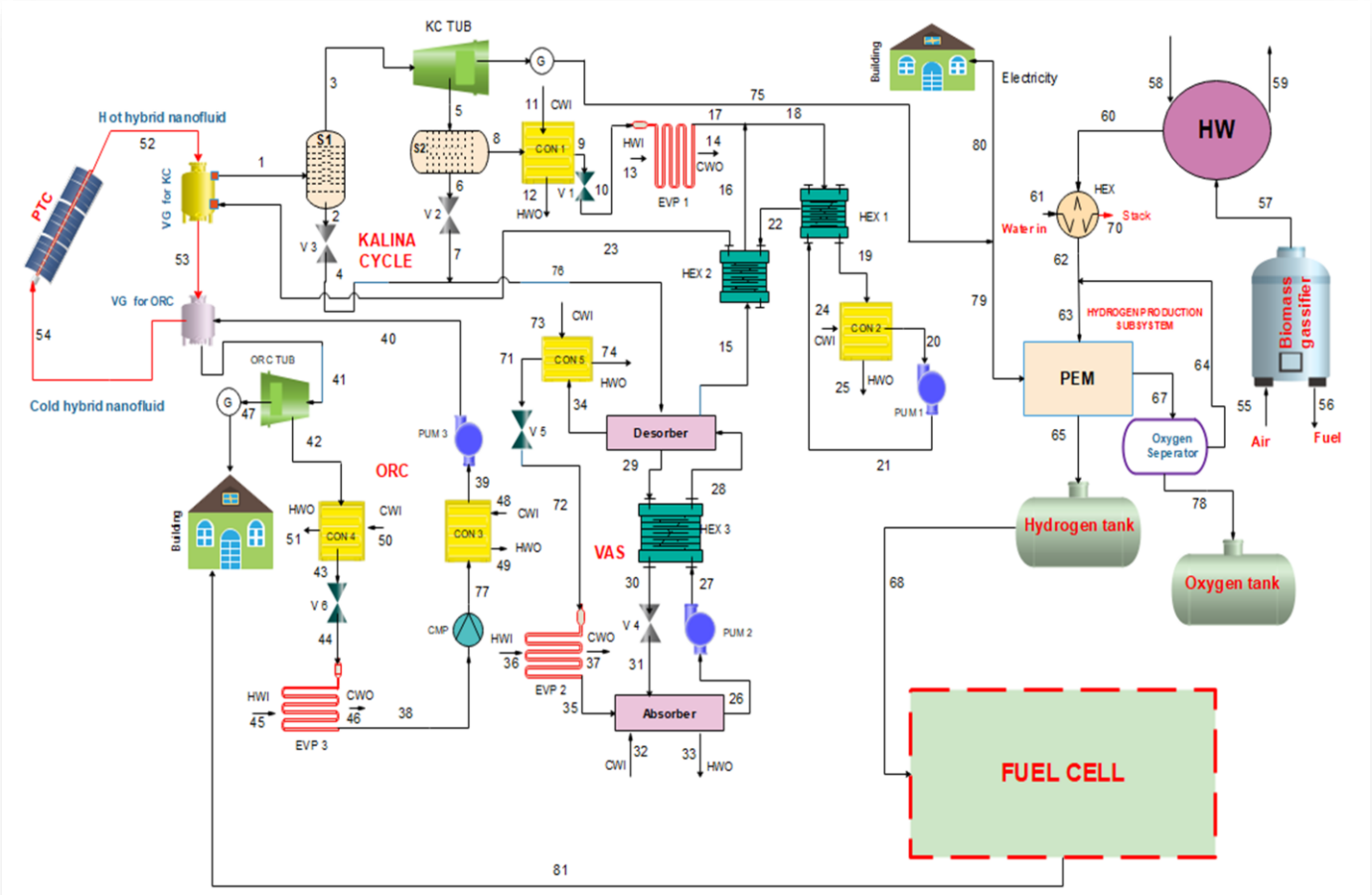

Fig. 2. Schematic diagram of the proposed solar-biomass-based multigeneration system.

2.1. Parabolic solar trough collector

The process begins with PTC, where a hybrid nanofluid, consisting of multi-walled carbon nanotubes and aluminium dioxide (MWCNT-Al_2O_3) mixed with therminol-VPI, serves as the heat transfer fluid. This fluid enters the solar collector as stream 54, where its energy is increased. The superheated fluid, now exiting as stream 52, first flows into the vapour generator associated with the Kalina cycle (VG for KC), transferring a portion of its thermal energy to the Kalina cycle's working fluid. After this, the fluid, now as stream 53, enters the vapour generator for the organic Rankine cycle (VG for ORC) and transfers additional heat energy to the ORC working fluid. Finally, the hybrid nanofluid returns to its initial state as stream 54, continuing the cycle uninterrupted.

2.2. Kalina cycle

The superheated steam-ammonia (NH_3-H_2O), which serves as the working fluid (stream 1) for the Kalina cycle, exits the vapour generator (VG for KC) and enters a separator (S1), where it splits into stream 2 and stream 3. Stream 2 is a high-pressure, high-temperature condensate that passes through a throttling valve, resulting in low-pressure stream 4. Stream 3, consisting of high-temperature and high-pressure steam-ammonia, expands through the Kalina turbine, converting some of its thermal energy into mechanical shaft work that drives an alternator to produce electricity. The expanded vapour (stream 5) then enters a second separator (S2), splitting into a lower-pressure condensate (stream 6) and another lower-pressure lower-temperature vapour (stream 8). Stream 6 is throttled into low-pressure stream 7, which then mixes uniformly with stream 4 to form stream 76. Stream 8 is condensed into a lower-temperature stream 9 and throttled into a lower-pressure stream 10, where it gains heat through the cooling process in the evaporator (EVP1). It exits as stream 17, mixing uniformly with stream 16 to form stream 18. This stream transfers its heat energy in the heat exchanger (HEX1), exits as stream 19, and further loses heat in the low-pressure condenser (CON2), emerging as stream 20. The pressure of stream 20 is increased by the pump (PUM1), resulting in stream 21, which gains heat in HEX1 to become stream 22 and then gains additional heat in heat exchanger (HEX2), exiting as stream 23, which returns to VG for KC, continuing the cycle in this manner.

2.3. Organic Rankine cycle

The working fluid (R245fa) in the ORC subsystem absorbs heat energy from the vapour generator (VG for ORC) and flows as stream 41 to the turbine, where it expands and converts part of its heat energy into mechanical shaft work, driving an alternator to generate electricity. The fluid then exits as stream 42 and enters the high-pressure condenser (CON4), where it loses some energy before exiting as stream 43. The pressure of stream 43 is further reduced through throttling, resulting in stream 44. It then gains heat energy through the cooling process in the evaporator (EVP3) and exits as stream 38, which is compressed by the compressor (CMP) into stream 77. Stream 77 flows into the low-pressure condenser (CON3), releases some heat energy, and exits as a low-temperature low-pressure stream 39. This stream is then pumped by pump (PUM3) back to the VG for ORC as stream 40, continuing the cycle in this sequence.

2.4. Vapour absorption system

The ammonia-water fluid (stream 76) from the Kalina cycle separators (S1 & S2) transfers heat to the lithium bromide water (LiBr-H_2O) solution in the desorber and exits as stream 15. When the weak LiBr-H_2O solution (stream 28) is heated, some of the absorbed water is released as vapour (stream 34). This process makes the remaining solution more concentrated (stream 29). The vapour from the generator/desorber is then condensed into a saturated liquid in a condenser (stream 34 to stream 71), where the rejected heat is used for space heating or hot water production. The condensed liquid is then throttled to a lower pressure, determined by setting the evaporator temperature to the saturation temperature and finding the corresponding saturation pressure. After throttling, the refrigerant is in a saturated liquid-vapour state (stream 72). It then passes through the evaporator, absorbing heat from the cooled or air-conditioned space. After the evaporator, the refrigerant goes to the absorber (stream 35). The strong solution from the desorber passes through a heat exchanger (HEX3), recovering some heat (stream 29 to stream 30) that was added in the desorber. This heat is then transferred to the incoming weak solution (stream 27 to stream 28). After the heat exchanger, the strong solution is throttled to the absorber's lower pressure (stream 31). The strong solution (stream 31) entering the absorber is cooled by releasing some heat into the atmosphere. The lower temperature increases its ability to absorb water vapour, so the vapour from the evaporator is absorbed to form a weak LiBr-H_2O solution (stream 26). This weak solution is then pumped to the desorber's higher pressure (stream 27) and passes through the heat exchanger (HEX3) to gain some heat (stream 28) before returning to the desorber. The cycle then repeats.

2.5. Biomass combustor, proton exchange membrane electrolyser and fuel cell

The heat released as flue gases (stream 57) from burning fuel derived from biomass gasification is directed to the hot water generating unit, where it transfers its heat to produce domestic hot water. The flue gases then exit (stream 60) into a heat exchanger (HEX), transferring energy to the incoming water (stream 61). The spent flue gases (stream 70) are expelled through the stack, while the heated water (stream 62) and hot water by-product (stream 64) from the proton exchange membrane (PEM) electrolyser mix uniformly as stream 63. Part of the electric power generated from the Kalina cycle (stream 79) is used in the electrolysis reaction to decompose the heated water (stream 63) in the PEM electrolyser, producing hydrogen (stream 65) for the H2 storage tank, and a mixture of oxygen and hot water (stream 67). This mixture is separated into oxygen (stream 78) for the O2 storage tank and hot water (stream 64), which is partially fed back into the PEM electrolyser. The chemical energy of the fuel, hydrogen (stream 68), and oxygen from the air is converted into electricity (stream 80) in the fuel cell unit through redox reactions.

3. Exergoeconomic Modelling and Analysis

The system's exergy-based costing is performed to determine the cost of the systems' products with regard to the components' cost, the lifetime of the system, and the number of hours of operation of the system. It also assists in quantifying the payback period and the economic losses accruable due to exergy destruction. This will assist in proper equipment sizing for reduction in economic losses during plant life. The components' purchase and equipment cost (PEC) are written as functions of their operating parameters, and are required to calculate the levelised cost rates during plant life operations in consonance with the cost equation balance. The PEC for the plant components can be found in related literature [23,24].

The general cost balance for a control volume is [25]:

$$\dot{C}_{q,k} + \sum_i \dot{C}_{i,k} + \dot{Z}_k = \sum_e \dot{C}_{e,k} + \dot{C}_{w,k}. \quad (1)$$

The terms in Eq. (1) represent the cost of heat transfer to the system's k^{th} component $\dot{C}_{q,k}$, the cost associated with the j^{th} sum of exergy streams to the system's k^{th} component $\sum_i \dot{C}_{i,k}$, and the levelised cost rate for the k^{th} component, $\dot{Z}_k$. The other terms are the cost associated with the j^{th} sum of exergy streams from the system's k^{th} component $\sum_e \dot{C}_{e,k}$, while the work associated with the k^{th} component in the system is denoted with the term $\dot{C}_{w,k}$.

The cost of the j^{th} stream is related to the cost of specific cost and the exergy, work or heat with the relationships:

$$\dot{C}_j = c_j \dot{E}x_j, \quad (2)$$

$$\dot{C}_{w,k} = c_w \dot{W}, \quad (3)$$

$$\dot{C}_{q,k} = c_q \dot{Q}. \quad (4)$$

The cost rate $\dot{Z}_k$ for the components is expressed as:

$$\dot{Z}_k = \frac{PECF \times CRF \times \phi}{N \times 3600}, \quad (5)$$

where PECF, CRF, and ϕ represent the purchase of equipment cost function, capital recovery factor, and maintenance factor, respectively.

The system's annual operational hours are denoted with *N*. Accordingly, the capital recovery factor is obtained with the relationship:

$$CRF = \frac{i|1+i|^n}{|1+i|^n - 1}, \quad (6)$$

where *n* is the estimated plant life in years.

Another exergy-related index is the cost of exergy of the product and fuel for the component. Detailed description of component cost of fuel and product is found in [26], but the principle is applied to this multigeneration system, and the balance is shown in Table 1.

The general relationships for evaluating the specific cost of product for the k^{th} component $c_{p,k}$ (\$/kJ), and that of fuel $c_{F,k}$ (\$/kJ), as well as the exergoeconomic factor, *f* are listed in Eqs. (7)–(9), respectively:

$$c_{P,k}\ (\$/\text{kJ}) = \frac{\dot{C}_{P,k}}{\dot{E}_{P,k}}, \quad (7)$$

$$c_{F,k}\ (\$/kJ) = \frac{\dot{C}_{F,k}}{\dot{E}_{F,k}}, \quad (8)$$

$$f = \frac{\dot{Z}_k}{\dot{Z}_k + \dot{C}_{D,k}}. \quad (9)$$

The cost of exergy destruction, which quantifies the economic loss attributed to inefficiencies, is expressed with the relationship:

$$\dot{C}_{D,k} = c_{P,k} E_{D,k}. \quad (10)$$

From Eq. (1), the cost balances and auxiliary relations are formulated for each of the components of the multigeneration system in Table 1.

3.1. Exergy based sustainability analysis

Exergy based sustainability analysis is used to analyse the availability of energy resources at low cost, with little or no effect on the environment [27]. The environmental effect is accounted for based on the magnitude of exergy destruction in the system, while the availability is based on the total net products from the system. The exergetic sustainability indicators considered in this study are exergy efficiency, exergy waste ratio, environmental effect factor and exergetic sustainability index were obtained from [28] and [29].

3.2. Sustainability indicators

The sustainability indicators are listed as a function of exergy efficiency, ψ_{plant}, exergy destruction ratio, $E_{D,\,Ratio}$, waste exergy ratio, Γ_w, environmental effect factor, Γ_{eef}, and exergetic sustainability index, θ_{esi}. The exergetic efficiency of the multigeneration plant is expressed as the ratio of exergy of product to fuel exergy [30]; the exergy waste ratio as the ratio of exergy waste to the chemical exergy of fuel. The ratio of total exergy destruction in the plant to the exergy of fuel is termed the exergy destruction ratio; while the environmental effect factor is the ratio of the waste exergy ratio to the exergy efficiency. Lastly, the exergetic sustainability index is the reciprocal of the environmental effect factor. The range of this index is between 0 and ∞ [28]. Mathematically, the indicators are expressed mathematically as:

$$\psi_{plant} = \frac{E_{x,product}}{E_{xfuel}}, \quad (11)$$

$$\Gamma_w = \frac{E_{waste}}{E_{x,fuel}}, \quad (12)$$

$$E_{D,Ratio} = \frac{\sum E_D}{E_{x,fuel}}, \quad (13)$$

$$\Gamma_{eef} = \frac{\Gamma_{w,e}}{\psi_{Plant}}, \quad (14)$$

$$\theta_{esi} = {}^{1}/_{\Gamma_{eef}}. \quad (15)$$

3.3. System optimisation

The optimisation of the system is performed to maximise the turbine work of the ORC and Kalina systems. With regard to the

Table 1. Summary of component costs and auxiliary equations.

Component	Component exergoeconomic balance	Auxiliary equation
Parabolic trough collector	$\dot{c}_{54} + \dot{c}_{\mathrm{Q_{solar}}} + \dot{Z}_{\mathrm{trough}} = \dot{c}_{52}$	Not applicable
Kalina VG	$\dot{c}_{52} + \dot{c}_{23} + \dot{Z}_{\mathrm{VG_{KC}}} = \dot{c}_{1} + \dot{c}_{53}$	$E_{53}\dot{c}_{52} - E_{52}\dot{c}_{53} = 0$
ORC VG	$\dot{c}_{53} + \dot{c}_{40} + \dot{Z}_{\mathrm{VG_{ORC}}} = \dot{c}_{54} + \dot{c}_{41}$	$E_{54}\dot{c}_{53} - E_{53}\dot{c}_{54} = 0$
ORC turbine	$\dot{c}_{41} + \dot{Z}_{\mathrm{ORC_{TURB}}} = \dot{c}_{42} + W_{\mathrm{TURB}} + W_{\mathrm{P_3}} + W_{\mathrm{ORC_{CMP}}}$	$\dot{E_{42}}c_{41} - E_{41}\dot{c}_{42} = 0;$ $W_{\mathrm{P_3}}\dot{c}_{\mathrm{W_{turb}}} - W_{\mathrm{turb}}\dot{c}_{\mathrm{W_{P_3}}} = 0;$ $W_{\mathrm{ORC_{CMP}}}\dot{c}_{\mathrm{W_{turb}}} - W_{\mathrm{turb}}\dot{c}_{\mathrm{W_{ORC_{CMP}}}} = 0.$
ORC CON 4	$\dot{c}_{42} + \dot{c}_{50} + \dot{Z}_{\mathrm{CON4}} = \dot{c}_{51} + \dot{c}_{43}$	$E_{43}\dot{c}_{42} - E_{42}\dot{c}_{43} = 0$
ORC valve (43, 44)	$\dot{c}_{43} + \dot{Z}_{\mathrm{VALVE}} = \dot{c}_{44}$	Not applicable
ORC EVP 3	$\dot{c}_{44} + \dot{Z}_{\mathrm{EVP3}} + \dot{c}_{45} = \dot{c}_{38} + \dot{c}_{46}$	$E_{46}\dot{c}_{45} - E_{45}\dot{c}_{46} = 0$
ORC Compressor	$\dot{c}_{38} + \dot{Z}_{\mathrm{ORC_{CMP}}} + \dot{c}_{\mathrm{ORC_{CMP}}} = \dot{c}_{77}$	Not applicable
ORC CON 3	$\dot{c}_{77} + \dot{c}_{48} + \dot{Z}_{\mathrm{CON3}} = \dot{c}_{49} + \dot{c}_{39}$	$E_{39}\dot{c}_{77} - E_{77}\dot{c}_{39} = 0$
ORC pump 3	$\dot{c}_{39} + \dot{Z}_{\mathrm{ORC_{P_3}}} + \dot{c}_{\mathrm{W_{P_3}}} = \dot{c}_{40}$	Not applicable
Kalina separator 1	$\dot{c}_{1} + \dot{Z}_{\mathrm{S_1}} = \dot{c}_{2} + \dot{c}_{3}$	$E_{3}\dot{c}_{2} - E_{2}\dot{c}_{3} = 0$
Kalina separator 2	$\dot{c}_{5} + \dot{Z}_{\mathrm{S_2}} = \dot{c}_{6} + \dot{c}_{8}$	$E_{8}\dot{c}_{6} - E_{6}\dot{c}_{8} = 0$
Kalina valve V3 (2,4)	$\dot{c}_{2} + \dot{Z}_{\mathrm{V_3}} = \dot{c}_{4}$	Not applicable
Kalina turbine	$\dot{c}_{3} + \dot{Z}_{\mathrm{KC_{TURB}}} = \dot{c}_{5} + \dot{c}_{\mathrm{W_{KC_{TURB}}}} + \dot{c}_{\mathrm{W_{P_1}}} + \dot{c}_{\mathrm{W_{P_2}}}$	$E_{5}\dot{c}_{3} - E_{3}\dot{c}_{5} = 0;$ $W_{\mathrm{P_1}}\dot{c}_{\mathrm{W_{kc,turb}}} - W_{\mathrm{kc,turb}}\dot{c}_{\mathrm{W_{P_1}}} = 0;$ $W_{\mathrm{P_2}}\dot{c}_{\mathrm{W_{P_1}}} - W_{\mathrm{P_1}}\dot{c}_{\mathrm{W_{P_2}}} = 0.$
Kalina valve, V2(6/7)	$\dot{c}_{6} + \dot{Z}_{\mathrm{V_2}} = \dot{c}_{7}$	Not applicable
Kalina CON 1	$\dot{c}_{8} + \dot{c}_{11} + \dot{Z}_{\mathrm{CON1}} = \dot{c}_{9} + \dot{c}_{12}$	$E_{9}\dot{c}_{8} - E_{8}\dot{c}_{9} = 0$
Kalina EVP 1	$\dot{c}_{10} + \dot{c}_{13} + \dot{Z}_{\mathrm{EVP1}} = \dot{c}_{17} + \dot{c}_{14}$	$E_{14}\dot{c}_{13} - E_{13}\dot{c}_{14} = 0$
Kalina CON 2	$\dot{c}_{19} + \dot{c}_{24} + \dot{Z}_{\mathrm{CON2}} = \dot{c}_{25} + \dot{c}_{20}$	$E_{20}\dot{c}_{19} - E_{19}\dot{c}_{20} = 0$
Kalina pump 1	$\dot{c}_{20} + \dot{c}_{\mathrm{W_{P_1}}} + \dot{Z}_{\mathrm{P_1}} = \dot{c}_{21}$	Not applicable
Kalina HEX 1	$\dot{c}_{18} + \dot{c}_{21} + \dot{Z}_{\mathrm{HEX1}} = \dot{c}_{22} + \dot{c}_{19}$	$E_{19}\dot{c}_{18} - E_{18}\dot{c}_{19} = 0$
Kalina HEX 2	$\dot{c}_{22} + \dot{c}_{15} + \dot{Z}_{\mathrm{HEX2}} = \dot{c}_{16} + \dot{c}_{23}$	$E_{23}\dot{c}_{22} - E_{22}\dot{c}_{23} = 0$
VAS desorber	$\dot{c}_{76} + \dot{c}_{28} + \dot{Z}_{\mathrm{Desorber}} = \dot{c}_{34} + \dot{c}_{29} + \dot{c}_{15}$	$E_{15}\dot{c}_{76} - E_{76}\dot{c}_{15} = 0;$ $E_{34}\dot{c}_{29} - E_{29}\dot{c}_{34} = 0.$
VAS CON. 5	$\dot{c}_{34} + \dot{c}_{73} + \dot{Z}_{\mathrm{CON5}} = \dot{c}_{71} + \dot{c}_{74}$	$E_{71}\dot{c}_{34} - E_{34}\dot{c}_{71} = 0$
VAS valve, V5 (71,72)	$\dot{c}_{71} + \dot{Z}_{\mathrm{V_5}} = \dot{c}_{72}$	Not applicable
VAS EVP 2	$\dot{c}_{76} + \dot{c}_{36} + \dot{Z}_{\mathrm{EVP2}} = \dot{c}_{35} + \dot{c}_{37}$	$E_{37}\dot{c}_{36} - E_{36}\dot{c}_{37} = 0$
VAS absorber	$\dot{c}_{35} + \dot{c}_{31} + \dot{c}_{32} + \dot{Z}_{\mathrm{Abs}} = \dot{c}_{26} + \dot{c}_{23}$	$(E_{33} - E_{32})\dot{c}_{26} - E_{26}(\dot{c}_{33} - \dot{c}_{32}) = 0$
VAS pump 2	$\dot{c}_{30} + \dot{c}_{\mathrm{W_{P_2}}} + \dot{Z}_{\mathrm{P_2}} = \dot{c}_{27}$	Not applicable
VAS valve 4	$\dot{c}_{30} + \dot{Z}_{\mathrm{V_4}} = \dot{c}_{31}$	Not applicable
VAS HEX 3	$\dot{c}_{27} + \dot{c}_{29} + \dot{Z}_{\mathrm{HEX3}} = \dot{c}_{28} + \dot{c}_{30}$	$E_{30}\dot{c}_{29} - E_{29}\dot{c}_{30} = 0$
Biomass combustor	$\dot{c}_{55} + \dot{c}_{56} + \dot{Z}_{\mathrm{BMC}} = \dot{c}_{57}$	Not applicable
Water heater (HW)	$\dot{c}_{57} + \dot{c}_{58} + \dot{Z}_{\mathrm{HW}} = \dot{c}_{60} + \dot{c}_{59}$	$E_{60}\dot{c}_{57} - E_{57}\dot{c}_{60} = 0$
HEX	$\dot{c}_{60} + \dot{c}_{61} + \dot{Z}_{\mathrm{HEX}} = \dot{c}_{70} + \dot{c}_{62}$	$E_{62}\dot{c}_{60} - E_{60}\dot{c}_{62} = 0$
PEM electrolyser	$\dot{c}_{76} + \dot{c}_{63} + \dot{Z}_{\mathrm{PEM}} = \dot{c}_{65} + \dot{c}_{67}$	$E_{67}\dot{c}_{65} - E_{65}\dot{c}_{67} = 0$

schematic of the energy system, the ORC turbine output is maximised with the objective function:

– maximise:

$$\dot{W}_{ORCT} = \dot{m}h|T_i, P_i| - h|s_i, P_o| = f|T_i, P_i, P_o|. \quad (16)$$

This is subject to the variables with constraints as:

$$T_{i,L} < T_i < T_{i,H}, \quad (17)$$

$$P_{i,L} < P_i < P_{i,H}, \quad (18)$$

$$P_{i,o} < P_o < P_{o,H}. \quad (19)$$

Equation (16) expresses the work output as a function of the enthalpy at the turbine inlet specified with turbine inlet tempera-

ature and pressure, and the exit enthalpy is defined with the entropy at the turbine inlet and the back pressure after expansion. The subscripts "*i*" and "*o*" respectively represent the inlet and outlet from the turbine, while "*L*" and "*H*" are for lower and higher operating limits.

Similarly, the turbine output from the Kalina system is maximised with the expression:

− maximise:

$$\dot{W}_{Kal.T} = \dot{m}h|T_i, P_i, q_i| - h|s_i, P_o| = f|T_i, P_i, P_o|, \quad (20)$$

where the quality of ammonium vapour at turbine inlet is denoted with q_i, and the objective function is subject to the variables with limits as:

$$T_{i,L} < T_i < T_{i,H}, \quad (21)$$

$$P_{i,L} < P_i < P_{i,H}, \quad (22)$$

$$P_{i,o} < P_o < P_{o,H}. \quad (23)$$

4. Results validation

To validate the thermodynamic simulation results for the proposed Multigeneration system, a suitable code was written in Engineering Equation Solver (EES) software [31] to compare the obtained findings to those in the literature. In this study, four case studies from the literature are chosen, and each is simulated in a constant situation. These case studies include the KC, ORC, VAS subsystem, and PEM electrolyser system. Validation for each case study is performed below.

4.1. Validation of Kalina cycle subsystem

In the first case study, a KC is selected from Parikhani et al.[32], and simulated under constant input parameters. In this simulation, some of the KC design input parameters of [32] were plugged into KC of the present work model. It can be expressed that the results of the current investigation properly corroborate the results of [32], with some improvements in performance indices. According to Table 2, a performance parameter (i.e. net output power) is selected, and the calculated value is compared with the literature. There is a good agreement between the obtained results in the present model and those reported in the literature.

Table 2. Model validation of the present work with Parikhani et al. [32] for the Kalina cycle subsystem.

Parameter	Reference [32]	Present work
System working fluid	Ammonia-water	Ammonia-water
Mass flow rate (kg/s)	2.917	2.917
Ammonia concentration at turbine outlet (%)	99.97	83.06
Turbine inlet temperature (°C)	160.2	160.2
Turbine inlet pressure (bar)	30	30
Turbine outlet pressure (bar)	2.986	2.986
Net power output (kW)	925.26	941.3

4.2. Validation of organic Rankine cycle subsystem

For the second case study, the results of the model for the organic Rankine cycle system are presented in Table 3. Assuming these input design parameters through the analysis of ORC, it can be stated that the results of the current investigation properly verify the results of Ozturk and Dincer [33], with some enhancements in the performance indices. From Table 3, a performance parameter (i.e. turbine power output) is selected, and the calculated value is compared with the literature. This comparison, of the different parameter, validates well with the literature.

Table 3. Model validation of the present work with Ozturk & Dincer [33] for the ORC generation subsystem.

Parameter	Reference [33]	Present work
System working fluid	Isobutane	Isobtane
Mass flow rate (kg/s)	34.24	34.24
Turbine inlet temperature (°C)	146.8	146.8
Turbine inlet pressure (bar)	32.5	32.5
Turbine outlet pressure (bar)	4.10	4.10
Turbine power output (kW)	2436	2437

4.3. Validation of vapour absorption subsystem

Presented in Table 4 is the third case study, which is the vapour absorption system (VAS). In the simulation, some of the VAS design input parameters of Karaca and Dincer [34] were substituted into VAS of the present work model. From Table 4, two performance parameters (i.e. evaporator cooling rate and energetic COP) are selected, and the calculated values are compared with the literature. This comparison, of the different parameters, agrees well with the literature.

Table 4. Model validation of the present work with Karaca & Dincer [34] for the VAS subsystem.

Parameter	Reference [34]	Present work
System working fluid	Ammonia-water	Ammonia-water
Mass flow rate (kg/s)	0.0089	0.0089
Pressure across the evaporator (bar)	4.62	4.62
VAS cooling rate (kW)	5.08	4.946
Energetic COP	0.96	0.9783

4.4. Validation of proton exchange membrane electrolyser subsystem

The fourth validation step is using a PEM electrolyser. In the mathematical modelling of the PEM electrolyser, the operating temperature is set at 90°C, the power supplied is 7.5 kW, and the oxygen and hydrogen pressures are fixed at 1 bar. Based on Table 5, a performance indicator (i.e., hydrogen production rate) is selected, and the calculated value is compared with the litera-

ture. It can be expressed that the results of the current investigation substantiate the results of Khanmohammadi et al. [35] as seen in Table 5, with some improvements in performance indices. A minor discrepancy is attributed to the different design operating conditions, like the unavailable or varying mass flow rate of water. Since the mass flow rate of water affects hydrogen production if it is insufficient, but once sufficient, the hydrogen flow rate increases with an increase in power supplied, as long as efficiency losses at high power are managed.

Table 5. Model validation of the present work with Khanmohammadi et al. [35] for PEM electrolyser.

Parameter	Reference [35]	Present work
Electrolyzer hot water mass flow rate (kg/s)	-	1.99
Electrolyzer temperature (°C)	90	90
Electrolyzer pressure (bar)	1	1
Hydrogen production rate (kg/h)	0.245	0.255

4.5. Validation of exergoeconomic performance

The final but not least significant step in validation is to use the comprehensive exergoeconomic and environmental results of a comparative system (Table 6).

Table 6. Exergoeconomic model validation of present work with Hashemian & Noorpoor [36] for the multigeneration system.

Parameter	Value	Present work
Total product cost rate ($/s)	0.83	0.798
Electricity cost rate ($/s)	0.0001	0.00016
Hydrogen cost rate ($/s)	0.0002	0.00021
Energy efficiency (%)	82.4	82.43

In the simulation, some of the system design input parameters of Hashemian & Noorpoor [36] were substituted into the present work model. From Table 6, six performance parameters (i.e. total product cost rate, electricity cost rate, cooling power cost rate and hydrogen cost rate) are selected, and the calculated values are compared with the literature. This comparison, of the different parameters, agrees well with the literature.

5. Results and discussion

5.1. Exergoeconomic results

The results of the exergoeconomic considerations of the plant as the main outcome of this study are presented in this section. It was conducted to determine the exergoeconomic factor of the plant, the cost related to exergy destruction, the total cost rate per second for the plant components, as well as the unit cost of products per energy. The unit cost of products was estimated separately for the electricity generation systems (ORC and Kalina cycle) only. This was based on the solution of the cost balance and auxiliary equations that yielded monetary quantification of the exergy streams at the state points. The cost parameters are summarised in Table 7. From the costs associated with the exergy stream and that of turbine work generated, the system's electricity cost from the Kalina cycle and ORC were computed as 0.04308 and 0.0245 USD/kWh, respectively. The calculated unit cost of electricity values translates to 69.12 ₦/kWh and 39.31 ₦/kWh based on the current exchange rate. These values are much desired when compared to the current electricity tariff of about 209.50 ₦/kWh (0.1306 USD/kWh) in Nigeria. The system's total cost of exergy destruction of 5.18 $/hr and equipment cost rate of 4.2 $/hr results in about 44.51% of the total exergoeconomic factor. Therefore, up to 55% of economic loss in the plant is related to the component's thermodynamic inefficiencies. The degree of each component contribution to economic loss is highlighted by the corresponding exergoeconomic factors in Table 7.

Table 7. Exergoeconomic results of the novel system.

Component	Equipment cost (USD)	Levelised equipment cost rate (USD/h)	Specific exergy cost of product (USD/GJ)	Cost of destruction (USD/h)	Exergoeconomic factor (%)
Biomass combustor	58124.00	1.368	0.000436	0.0009464	99.93
Kalina condenser 1	2444.00	0.05755	0.006077	0.0309744	65.01
Kalina condenser 2	1953.00	0.04598	0.003294	0.0207000	68.96
Kalina evaporator 1	1694.00	0.03988	0.001944	0.1502640	20.97
Kalina HEX 1	1533.00	0.0361	0.01521	0.0638640	36.11
Kalina HEX 2	955.60	0.0225	0.009738	0.1139400	16.49
Kalina pump 1	25.19	0.000593	0.01203	0.0000581	91.08
Kalina separator 1	805.80	0.01897	0.001355	0.0228060	45.41
Kalina separator 2	805.80	0.01897	0.001562	0.0002475	98.71
Kalina turbine	30940.00	0.7285	0.01197	0.0000000	100.00
Kalina valve 1	161.60	0.003805	0.001944	0.0131328	22.46
Kalina valve 2	161.60	0.003805	0.01112	0.0005753	86.87
Kalina valve 3	330.20	0.007775	0.003261	0.0336276	18.78
Kalina vapour generator	5635.00	0.1327	0.000567	0.0434160	75.35
ORC compressor	1374.00	0.03235	0.007699	0.0521640	38.28
ORC condenser 3	1137.00	0.02678	0.000603	1.0483200	2.49

Table 7 continued. Exergoeconomic results of the novel system.

Component	Equipment cost (USD)	Levelised equipment cost rate (USD/h)	Specific exergy cost of product (USD/GJ)	Cost of destruction (USD/h)	Exergoeconomic factor (%)
ORC condenser 4	1311.00	0.03087	0.01424	0.2283840	11.91
ORC evaporator 3	1311.00	0.03087	0.002451	0.1681920	15.51
ORC pump	29.79	0.000701	0.006892	0.0001922	78.49
ORC turbine	41103.00	0.9677	0.006822	0.0924120	91.28
ORC vapour generator	1423.00	0.03351	0.000567	0.0434160	43.56
ORC valve	140.80	0.003315	0.02226	0.2611080	1.25
PEM electrolyser	2843.00	0.06694	0.00261	0.0305388	68.67
PEM HEX	1137.00	0.02678	0.002187	0.3209040	7.70
Trough collector	10026.00	0.2361	0.000113	0.0000000	100.00
VAS absorber	1368.00	0.0322	0.0124	0.5958000	5.13
VAS condenser 5	1137.00	0.02678	0.02249	0.0085500	75.80
VAS desorber	1694.00	0.03988	0.003571	0.2546280	13.54
VAS evaporator 2	1254.00	0.02952	0.002666	0.0021600	93.18
VAS HEX3	1137.00	0.02678	0.006502	0.3054960	8.06
VAS pump	3.63	8.53E-05	0.01119	0.0101664	0.83
VAS valve 4	166.80	0.003926	0.01498	0.0808200	4.63
VAS valve 5	166.80	0.003926	0.002666	0.7822800	0.50
Water heater	2202.00	0.05185	0.002815	0.4010400	11.45
Total	176533.61	4.155991	0.226233	5.1811234	44.51

5.2. Sensitivity analysis

The effect of some key thermodynamic parameters on the key performance criteria of the system is investigated in this section. Figure 2 reveals a significant relationship between the turbine inlet temperature, pressure, and total cost rate. Specifically, a 20°C increase in turbine inlet temperature from 140°C to 160°C yields a 3.8% rise in total cost rate, while a 66.7% increase in turbine inlet pressure from 15 bar to 25 bar results in a 3.5% cost rate escalation. These findings underscore the intricate balance between thermodynamic efficiency, heat transfer rates, and component costs.

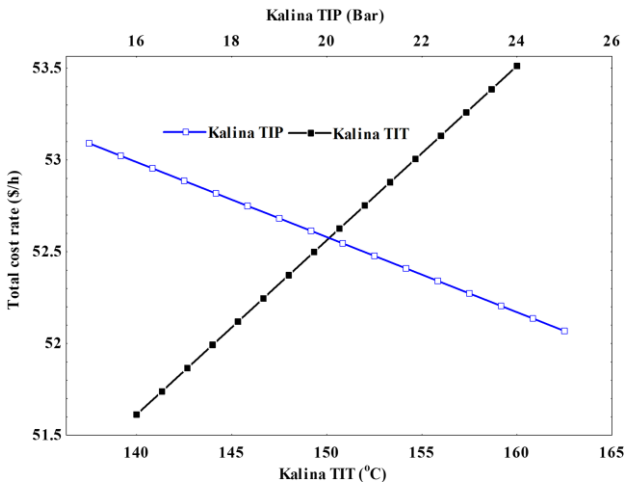

Fig. 2. Variation of the Kalina turbine inlet temperature and pressure with the total cost rate.

The system's configuration, comprising the Kalina cycle, organic Rankine cycle, and vapour absorption system, exhibits sensitivity to turbine inlet conditions, emphasising the importance of optimising operating parameters to mitigate increased costs.

Figure 3 shows the relationship between the ORC turbine inlet temperature and pressure and the multigeneration energy system's cost rate. As the inlet temperature increases from 125°C to 160°C, the total cost rate remains relatively stable, fluctuating between $52.45 and $53.65. Conversely, the inlet pressure exhibits a more pronounced impact, with the cost rate escalating from $53.35 at 22 bar to $52.25 at 27 bar. This disparity suggests that optimising turbine inlet pressure may yield greater cost savings. Notably, the system demonstrates thermal efficiency resilience within the 125°C−155°C temperature range, but experiences a slight cost increase beyond 155°C.

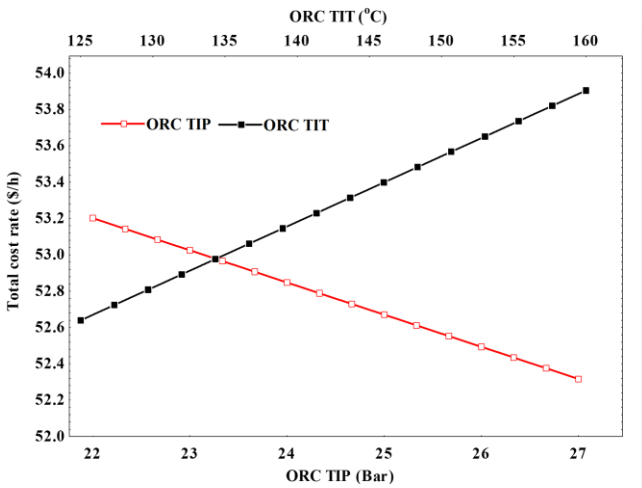

Fig. 3. Variation of the ORC turbine inlet temperature and pressure with the total cost rate.

Figure 4 reveals a positive linear relationship between the parabolic trough collector (PTC) area and total cost rate, with a minimal increase of approximately 0.4% per 5 m² increase in the PTC area. As the PTC area expands from 20 m² to 45 m², the total cost rate rises from \$52.61/h to \$52.83/h, demonstrating efficient scaling and economies of scale. This trend is attributed to reduced costs per unit area, efficient heat collection, linear scaling, and fixed costs associated with system components. The system's configuration benefits from increased heat input and maintains relatively consistent thermal efficiency.

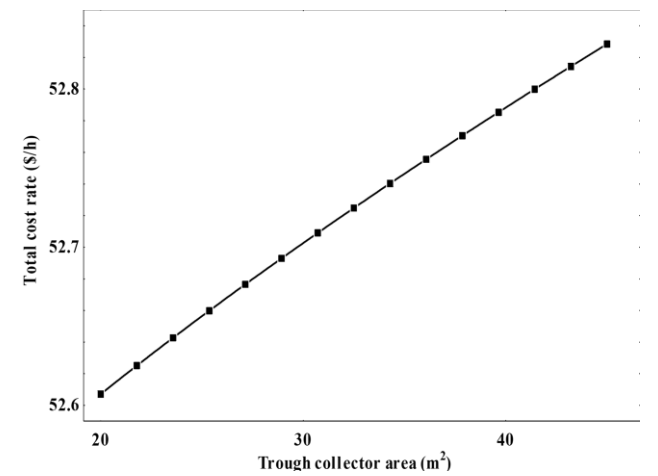

Fig. 4. The effect of trough collector area on the total cost rate.

Figure 5 reveals a trade-off between the total cost rate and total plant exergy efficiency as the parabolic trough collector (PTC) mass flow rate increases from 2 kg/s to 3.5 kg/s. The total cost rate rises linearly by 4.7% from \$50.67/h to \$53.15/h, while the total plant exergy efficiency decreases non-linearly by 14.6% from 80.52% to 65.6%. The efficiency drop accelerates beyond 2.75 kg/s, highlighting the importance of balancing cost and efficiency. This trend is attributed to increased heat transfer and thermal losses, pumping power requirements, and system design limitations.

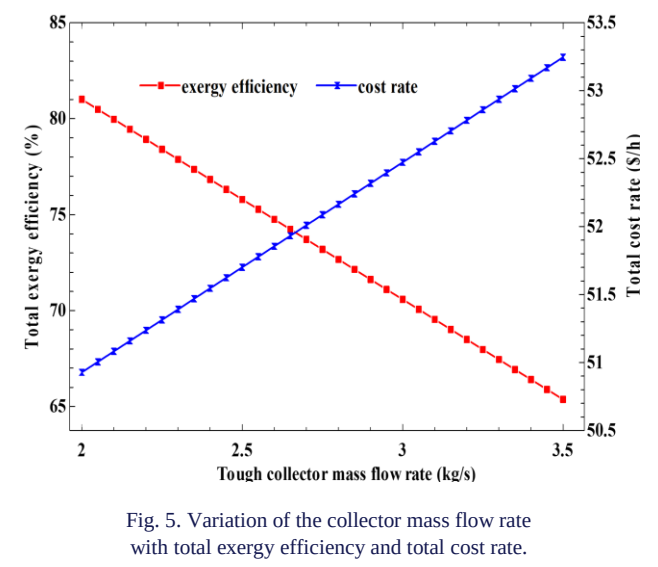

Fig. 5. Variation of the collector mass flow rate with total exergy efficiency and total cost rate.

Figure 6 shows the trade-off between the total cost rate and total efficiency as the parabolic trough collector (PTC) mass flow rate increases from 20 m² to 45 m². The total cost rate rises linearly by 4.8% from \$50.67/h to \$53.15/h, while the total efficiency decreases non-linearly by 18.5% from 80.52% to 65.6%. This decline is attributed to increased thermal losses, reduced heat recovery, and decreased organic Rankine cycle and vapour absorption system efficiencies.

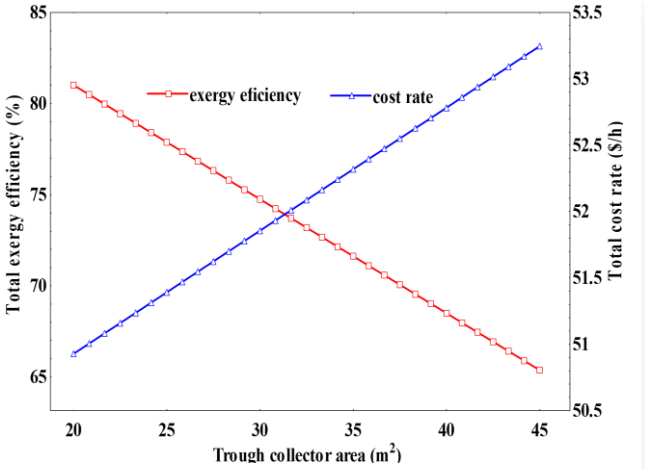

Fig. 6. Variation of the collector area with total exergy efficiency and total cost rate.

The efficiency drop accelerates beyond 30 kg/s, highlighting a critical mass flow rate threshold. Optimising the PTC mass flow rate, component selection, and system design can mitigate this efficiency decrease, achieving a more favourable cost-efficiency balance in the multigeneration energy system.

5.3. Optimisation results

The optimisation was performed with regards to the optimum selection of operating parameters for the ORC and Kalina turbines. The work output from these turbines was optimised subject to the ideal temperature and pressure mix within the thermodynamic operation domain. The ORC work output optimisation results are shown in Fig. 7 after 2152 iterations performed with 64 genetic algorithm generations. The optimum work produced from the ORC turbine was obtained as 47.97 kJ/kg at a turbine inlet temperature and pressure of 140°C and 25.7 bar, respectively. The turbine back pressure (TBP) was optimised to 2.003 bar. The optimum parameters for the ORC are summarised in Table 8. The surface plot of the optimum turbine work with regards to TIP and TBP in the optimisation search space is also shown in Fig. 8.

Table 8. ORC optimum operating parameters.

Parameter	Limits	Optimum value	Unit
Turbine work	–	47.97	kJ/kg
TIT	110 –140	140	°C
TIP	15 – 30	25.7	bar
TBP	2 – 6	2.003	bar

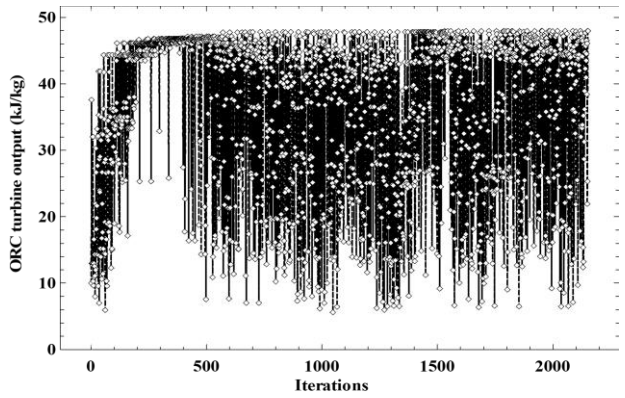

Fig. 7. ORC optimum work output.

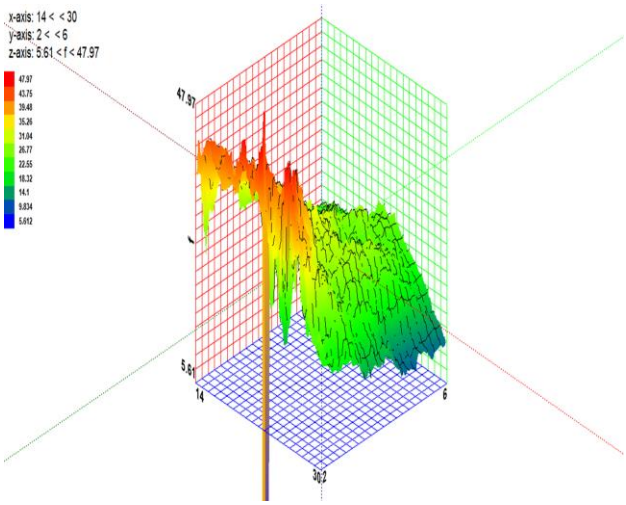

Fig. 8. Surface plot of the optimum turbine work with regards to TIP and TBP.

Similar optimisation results for the Kalina system are shown in Fig. 9. Several optimization runs yielded the maximum turbine work outputs of approximately 435 kJ/kg. However, the operating turbine inlet temperature and pressure tended towards the upper constraints, while the pressure after expansion tended towards the lower bound. The optimum parameters are shown in Table 4, while all iterations involving the objective function and decision variables are well documented.

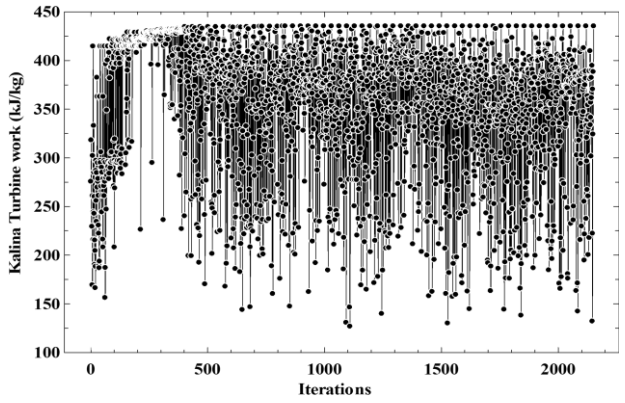

Fig. 9. KC optimum work output.

Table 6. Kalina system optimum operating parameters.

Parameter	Limits	Optimum value	Unit
Turbine work	–	435.3	kJ/kg
TIT	120 – 160	159.1	°C
TIP	15 –30	30	bar
TBP	2 – 8	2.006	bar

5.4. Exergetic sustainability analysis of the system

The results of the sustainability index of the system were found with regards to the total system output and gross exergy destruction in the plant. At design condition, the system has an exergy efficiency of 52.2%, total exergy destruction of 963.3 kW, and total product of 964.9 kW. Accordingly, the system's exergy sustainability index was 1.002. This shows that the system's output is slightly higher than the total exergy destruction in the system, although there were massive gross exergy destructions, especially in the parabolic trough collector, due to the high temperature gradient between the PTC surface and the surroundings. An improvement on the exergetic sustainability index can be achieved with a reduction in the net exergy destruction through variation in operating parameters. One such parameter is the ambient temperature. The results in Fig. 10 show that high ambient temperatures will result in ESI. Interestingly, an optimum ambient temperature exists at about 297.4 K where the system's ESI can reach 1.00.

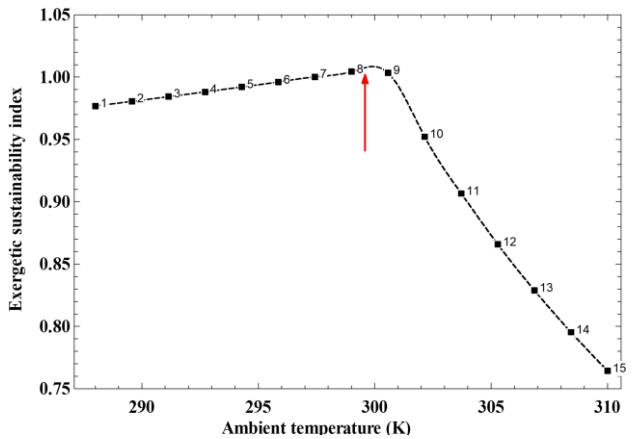

Fig. 10. Effect of ambient temperature on the system's ESI.

6. Conclusions

The present study performed an exergoeconomic investigation and optimisation of a solar-biomass tri-evaporator multi-generation plant equipped with a fuel cell and a proton exchange membrane. The system includes a parabolic trough collector powered by the sun, which is the primary energy source for the integrated energy system; a Kalina system that provides power and cooling; an organic Rankine cycle (ORC) for power and cooling; a vapour absorption system for refrigeration; and a proton exchange membrane (PEM) electrolyzer for hydrogen production supported by a biomass combustor. A sensitivity analy-

sis is carried out to examine the effect of various design factors. The main conclusions are that:

- The system's electricity cost from the Kalina and ORC were computed as 0.04308 USD/kWh and 0.0245 USD/kWh, respectively, with a total system cost of 176533 USD. The system's total cost of exergy destruction of 5.18 $/h and equipment cost rate of 4.2 $/h results in about 44.51% of the total exergoeconomic factor.
- The calculated unit cost of electricity values translates to 69.12 ₦/kWh and 39.31 ₦/kWh based on the current exchange rate. These values are much desired when compared to the current electricity tariff of about 209.50 ₦/kWh (0.1306 USD/kWh) in Nigeria.
- The optimum power generation from the ORC turbine was obtained as 47.97 kW at a turbine inlet temperature and pressure of 140°C and 25.7 bar, respectively. The turbine back pressure (TBP) was optimised to 2.003 bar.
- The optimum power generation from the Kalina turbine was obtained as 435 kW at a turbine inlet temperature and pressure of 159.1°C and 30 bar, respectively, and TBP of 2.006 bar.
- An optimum ambient temperature exists at about 297.4 K where the system's ESI can reach 1.00.

References

[1] Jamali, D.H., & Noorpoor, A. (2019). Optimization of a novel solar-based multi-generation system for waste heat recovery in a cement plant. *Journal of Cleaner Production*, 240, doi: 10.1016/j.jclepro.2019.117825

[2] Hosseini, S.S., Mehrpooya, M., Alsagri, A.S., & Alrobaian, A.A. (2019). Introducing, evaluation and exergetic performance assessment of a novel hybrid system composed of MCFC, methanol synthesis process, and a combined power cycle. *Energy Conversion and Management*, 197, doi: 10.1016/j.enconman.2019.111878

[3] Alsagri, A.S, Chiasson, A., & Aljabr, A. (2018). Performance Comparison and Parametric Analysis of sCO2 Power Cycles Configurations. *ASME 2018 International Mechanical Engineering Congress and Exposition*. V06BT08A007. November 9–15, Pittsburgh, Pennsylvania, USA. doi: 10.1115/imece2018-86843

[4] Aghbashlo, M., Tabatabaei, M., Hosseini, S.S., & Younesi, H. (2016). Najafpour G. Performance analysis of a continuous bioreactor for ethanol and acetate synthesis from syngas via Clostridium ljungdahlii using exergy concept. *Clean Technologies and Environmental Policy*, 18(3), 853–865. doi: 10.1007/s10098-015-1061-3

[5] Yuksel, Y.E., & Ozturk, M. (2016). Thermodynamic and thermoeconomic analyses of a geothermal energy based integrated system for hydrogen production. *International Journal of Hydrogen Energy*, 42(4), 2530–2546. doi: 10.1016/j.ijhydene.2016.04.172

[6] Dincer, I. (2000). Renewable energy and sustainable development: a crucial review. *Renewable and Sustainable Energy Reviews*. 4(2), 157–175. doi: 10.1016/s1364-0321(99)00011-8

[7] Leiva-Illanes, R., Escobar, R., Cardemil, J., Alarcón P., & Diego, C. (2018). Comparison of the levelized cost and thermoeconomic methodologies – Cost allocation in a solar polygeneration plant to produce power, desalted water, cooling and process heat. *Energy Conversion and Management*, 168: 215–229. doi: 10.1016/j.enconman.2018.04.107

[8] Kopp, M., Coleman, D., Stiller, C., Scheffer, K., Aichinger, J., & Scheppat, B. (2017). Energiepark Mainz: Technical and economic analysis of the worldwide largest Power-to-Gas plant with PEM electrolysis. *International Journal of Hydrogen Energy*, 42(19), 13311–13320. doi: 10.1016/j.ijhydene.2016.12.145

[9] Pourrahmani, H., & Moghimi, M. (2019). Exergoeconomic analysis and multi-objective optimization of a novel continuous solar-driven hydrogen production system assisted by phase change material thermal storage system. *Energy*, 189, 116170. doi: 10.1016/j.energy.2019.116170

[10] Ahmadi, P., Dincer, I., & Rosen, M.A. (2014). Thermoeconomic multi-objective optimization of a novel biomass-based integrated energy system. *Energy*, 1−13. doi: 10.1016/j.energy.2014.01.085

[11] Calise, F., d'Accadia, M.D., Macaluso, A., Piacentino, A., & Vanoli, L. (2016). Exergetic and exergoeconomic analysis of a novel hybrid solar–geothermal polygeneration system producing energy and water. *Energy Conversion and Management*, 115, 200−220. doi: 10.1016/j.enconman.2016.02.029

[12] Baghernejad, A., Yaghoubi, M., & Jafarpur, K. (2016). Exergoeconomic optimization and environmental analysis of a novel solar-trigeneration system for heating, cooling and power production purpose. *Solar Energy*, 134, 165−179. doi: 10.1016/j.solener.2016.04.046

[13] Moharamian, A., Soltani, S., Rosen, M.A., & Mahmoudi, S.M. (2017). Exergoeconomic and thermodynamic analyses of an externally fired combined cycle with hydrogen and injection to the combustion chamber. *International Journal of Hydrogen Energy*, 43(2), 781–792. doi: 10.1016/j.ijhydene.2017.11.136

[14] Khalid, F., Dincer, I., & Rosen, M.A. (2017). Thermoeconomic Analysis of a Solar-Biomass Integrated Multigeneration System for a Community. *Applied Thermal Engineering*, 120, 645−653. doi: 10.1016/j.applthermaleng.2017.03.040

[15] Khanmohammadi, S., Heidarnejad, P., Javani, N., & Ganjehsarabi, H. (2017). Exergoeconomic analysis and multi objective optimization of a solar based integrated energy system for hydrogen production. *International Journal of Hydrogen Energy*, 42(33), 21433−21453. doi: 10.1016/j.ijhydene.2017.02.105

[16] El-Emam, R.S., & Dincer, I. (2018). Investigation and assessment of a novel solar-driven integrated energy system. *Energy Conversion and Management*, 158, 246–255. doi: 10.1016/j.enconman.2017.12.062

[17] Khanmohammadi, S., Saadat-Targhi, M., Al-Rashed, A.A., & Afrand, M. (2019). Thermodynamic and economic analyses and multi-objective optimization of harvesting waste heat from a biomass gasifier integrated system by thermoelectric generator. *Energy Conversion and Management*, 195, 1022–1034. doi: 10.1016/j.enconman.2019.05.075

[18] Behzadi, A., Habibollahzade, A., Zare, V., & Ashjaee, M. (2019). Multi-objective optimization of a hybrid biomass-based SOFC/GT/double effect absorption chiller/RO desalination system with CO_2 recycle. *Energy Conversion and Management*, 181, 302–318. doi: 10.1016/j.enconman.2018.11.053

[19] Anvari, S., Mahian, O., Taghavifar, H., Wongwises, S., & Desideri, U. (2020). 4E analysis of a modified multigeneration system designed for power, heating/cooling, and water desalination. *Applied Energy*, 270, 115107. doi: 10.1016/j.apenergy.2020.115107

[20] Abdelhay, A.O., Fath, H.E.S., & Nada, S.A. (2020). Solar-driven polygeneration system for power, desalination, and cooling. *Energy*, 198, 117341. doi.: 10.1016/j.energy.2020.117341

[21] Alirahmi, S.M., Rostami, M., & Farajollahi, A.H. (2020). Multi-criteria design optimization and thermodynamic analysis of a novel multi-generation energy system for hydrogen, cooling, heating, power, and freshwater. *International Journal of Hydrogen Energy*, 45(30), 15047–15062. doi: 10.1016/j.ijhydene.2020.

03.235

[22] Khan, M.S., Abid, M., Bashir, M.A., Amber, K.P., Khanmohammadi, S., & Yan, M. (2021). Thermodynamic and exergoeconomic analysis of a novel solar-assisted multigenerational system utilizing high temperature phase change material and hybrid nanofluid. *Energy Conversion and Management*, 236, 113948 doi: 10.1016/j.enconman.2021.113948

[23] Genc, G.C., Celik, M., & Genc, M.S. (2012). Cost analysis of wind-electrolyzer fuel cell system for energy demand in Pınarbaşı-Kayseri. *International Journal of Hydrogen Energy*, 37 (17), 12158-12166. doi: 10.1016/j.ijhydene.2012.05.058

[24] Ahmadi, P., Dincer, I., & Rosen M.A. (2013). Energy and exergy analyses of hydrogen production via solar-boosted ocean thermal energy conversion and PEM electrolysis. *International Journal of Hydrogen Energy*, 38(4), 1795−1805. doi: 10.1016/j.ijhydene. 2012.11.025

[25] Bejan, A., Tsatsaronis, G., & Moran, M. (1996). Thermal design and optimization. John Wiley & Sons, Inc., New York.

[26] Tsatsaronis, G., & Lin, L. (1990). On exergy costing in exergoeconomics. *Proceedings of computer-aided energy systems analysis*, American Society of Mechanical Engineers, 25-30 Nov., Dallas, TX, United States.

[27] Aydin, H. (2013). Exergetic sustainability analysis of LM6000 gas turbine power plant with steam cycle. *Energy*, 57, 766–774. doi: 10.1016/j.energy.2013.05.018

[28] Midilli, A., & Dincer, I. (2009). Development of some exergetic parameters for PEM fuel cells for measuring environmental impact and sustainability. *International Journal of Hydrogen Energy*, 34(9), 3858–3872. doi: 10.1016/j.ijhydene.2009.02.066

[29] Midilli, A., Inac, S., & Ozsaban, M. (2017). Exergetic sustainability indicators for a high-pressure hydrogen production and storage system. *International Journal of Hydrogen Energy*, 42(33), 21379–21391. doi: 10.1016/j.ijhydene.2017.04.299

[30] Kotas, T.J. (1995). The Exergy Method of Thermal Plant Analysis. Reprint Edition, Krieger Publishing Company, Malabar, Florida.

[31] Engineering Equation Solver (EES), 2013. Klein, S.A. from fchart.com/ees/.

[32] Parikhani, T., Gholizadeh, T., Ghaebi, H., Sadat, S.M., & Sarabi, M. (2018). Exergoeconomic optimization of a novel multigeneration system driven by geothermal heat source and liquefied natural gas cold energy recovery. *Journal of Cleaner Production*. doi: 10.1016/j.jclepro.2018.09.181

[33] Ozturk, M., & Dincer, I. (2013). Thermodynamic analysis of a solar-based multi-generation system with hydrogen production. *Applied Thermal Engineering* , 51(42), 1235−1244. doi: 10.1016/ j.applthermaleng.2012.11.0

[34] Karaca, A.E., & Dincer, I. (2020). A new integrated solar energy based system for residential houses. *Energy Conversion and Management*, 221, 113112. doi: 10.1016/j.enconman.2020. 113112

[35] Khanmohammadi, S., Heidarnejad, P., Javani, N., & Ganjehsarabi, H. (2017). Exergoeconomic analysis and multi objective optimization of a solar based integrated energy system for hydrogen production. *International Journal of Hydrogen Energy*, 42(33), 21443–21453. doi: 10.1016/j.ijhydene.2017.02.105

[36] Hashemian, N., & Noorpoor, A. (2019). Assessment and multicriteria optimization of a solar and biomass-based multi-generation system: Thermodynamic, exergoeconomic and exergoenvironmental aspects. *Energy Conversion and Management*, 195, 788–797. doi: 10.1016/j.enconman.2019.05.039